Biochem. J. (2008) **410**, 463–472 (Printed in Great Britain) doi:10.1042/BJ20070559

online data

Acyl-CoA-binding protein (ACBP) localizes to the endoplasmic reticulum and Golgi in a ligand-dependent manner in mammalian cells

Jesper S. HANSEN*, Nils J. FÆRGEMAN*, Birthe B. KRAGELUND† and Jens KNUDSEN*[1]

*Department of Biochemistry and Molecular Biology, University of Southern Denmark, Campusvej 55, DK-5230 Odense M, Denmark, and †Department of Molecular Biology, Ole Maaløes Vej 5, DK-2200 Copenhagen N, Denmark

In the present study, we microinjected fluorescently labelled liver bovine ACBP (acyl-CoA-binding protein) [FACI-50 (fluorescent acyl-CoA indicator-50)] into HeLa and BMGE (bovine mammary gland epithelial) cell lines to characterize the localization and dynamics of ACBP in living cells. Results showed that ACBP targeted to the ER (endoplasmic reticulum) and Golgi in a ligand-binding-dependent manner. A variant Y28F/K32A-FACI-50, which is unable to bind acyl-CoA, did no longer show association with the ER and became segregated from the Golgi, as analysed by intensity correlation calculations. Depletion of fatty acids from cells by addition of FAFBSA (fatty-acid-free BSA) significantly decreased FACI-50 association with the Golgi, whereas fatty acid overloading increased Golgi association, strongly supporting that ACBP associates with the Golgi in a ligand-dependent manner. FRAP (fluorescence recovery after photobleaching) showed that the fatty-acid-induced targeting of FACI-50 to the Golgi resulted in a 5-fold reduction in FACI-50 mobility. We suggest that ACBP is targeted to the ER and Golgi in a ligand-binding-dependent manner in living cells and propose that ACBP may be involved in vesicular trafficking.

Key words: acyl-CoA-binding protein (ACBP), confocal microscopy, endoplasmic reticulum, Golgi, trafficking, two-photon excitation fluorescence recovery after photobleaching (FRAP).

INTRODUCTION

ACBP (acyl-CoA-binding protein) is a highly conserved protein from protozoa to humans [1], which suggests that the protein is required for very basic functions conserved throughout the eukaryotic kingdom. Our understanding of the function of ACBP is still incomplete. *In vitro* studies have shown that ACBP desorbs acyl-CoA esters embedded in immobilized synthetic lipid membranes and donates acyl-CoA to β-oxidation in mitochondria or glycerolipid synthesis in microsomes [2,3], suggesting that ACBP acts as an acyl-CoA transporter. Depletion of the ACBP homologue, Acb1p, from the yeast *Saccharomyces cerevisiae* results in strongly reduced growth, accumulation of large amounts of cytoplasmic vesicles and multilayered plasma membranes and fragmented vacuoles [4]. The vacuoles isolated from the Acb1p-depleted strain lack important SNARE (soluble *N*-ethylmaleimide-sensitive fusion protein-attachment protein receptor) proteins and are unable to undergo homoeotypic fusion [4]. This indicates that ACBP in the yeast may play a role in vesicular trafficking. The Acb1p-depleted strain also shows strongly reduced ceramide levels [5], indicating also a role for ACBP in long-chain base synthesis and/or fatty acid elongation. The finding that a *Caenorhabditis elegans* ACBP domain protein MAA-1 is required for vesicular transport between the plasma membrane and Golgi complex [6] further suggests a role of the ACBP domain in vesicular trafficking. Experimental evidence also suggests that ACBP plays a role in the regulation of HNF-4α (hepatocyte nuclear factor-4α) [7] and further interacts with the $GABA_{A\alpha1}$ (γ-aminobutyric acid Aα1) receptor subunit in rabbit Müller cells [8]. Finally, ACBP has been shown to augment Bid-induced mitochondrial damage and cell death by activating μ-calpain [9].

Knowledge of the intracellular localization and movement of ACBP in living cells would be of great value in assigning a function to specific processes. Numerous *in vitro* studies have been carried out to characterize the cellular localization of the basal 82–92-residue ACBP (see [10] for a review). Subcellular fractionation and immunohistochemical studies at the level of electron microscopy report that ACBP can be found in the cytosol associated with the smooth ER (endoplasmic reticulum), Golgi, the outer membrane of mitochondria and around large cytoplasmic vesicles [11–20]. Studies with the hornworm *Manduca sexta* intestinal columnar cells and prothoracic gland ecdystereogenic cells [19] and 3T3-L1 cells [21] show that ACBP, in addition to being present in the cytosol, also appears in the nucleus.

The existing experimental results draw a very confused picture of the possible intracellular localization of ACBP and do not add to our understanding of the biological function of the protein. A further complication in the interpretation of the immunohistochemical and immunofluorescence data is that ACBP cannot be fixed by conventional protein-denaturizing methods. After denaturation with trichloroacetic acid, ACBP readily re-dissolves in buffered solutions at neutral pH (J.S. Hansen, N.J. Færgeman, B.B. Kragelund and J. Knudsen, unpublished work). Hence, incomplete fixing of ACBP will result in loss of ACBP during the immunostaining process.

To circumvent the above-mentioned problems, we have in the present study visualized the cellular localization of ACBP in living HeLa and BMGE (bovine mammary gland epithelial) cells by using microinjection of fluorescently labelled bovine L-ACBP

Abbreviations used: ACBP, acyl-CoA-binding protein; badan, 6-bromoacetyl-2-dimethylaminonaphthalene; BMGE, bovine mammary gland epithelial; BODIPY®, 4,4-difluoro-4-bora-3a,4a-diaza-*s*-indacene; DAPI, 4′,6-diamidino-2-phenylindole; DMEM, Dulbecco's modified Eagle's medium; $DMEM_{pen/strep}$, DMEM with 50 units/ml penicillin and 50 μg/ml streptomycin; DOPC, 1,2-dioleoyl-*sn*-3-glycerophosphocholine; ER, endoplasmic reticulum; FACI, fluorescent acyl-CoA indicator; FAFBSA, fatty-acid-free BSA; FBS, foetal bovine serum; FRAP, fluorescence recovery after photobleaching; GFP, green fluorescent protein; GP, generalized polarization; ICA, intensity correlation analysis; ICQ, intensity correlation quotient; L-ACBP, liver-type ACBP; NA, numerical aperture; OA, oleic acid; PDM, product of the differences from the mean; SNARE, soluble *N*-ethylmaleimide-sensitive fusion protein-attachment protein receptor.

[1] To whom correspondence should be addressed (email jkk@bmb.sdu.dk).

(liver-type ACBP) [FACI-50 (fluorescent acyl-CoA indicator-50)] [22]. The results show that ACBP localizes to the ER and Golgi complex in a ligand-dependent manner.

EXPERIMENTAL

Reagents

Nuclon angle-necked T_{75} culture flasks with filter caps were from Nunc A/S (Roskilde, Denmark). Uncoated 50 mm glass-bottom culture dishes were from MatTek (Ashland, MA, U.S.A.). DMEM (Dulbecco's modified Eagle's medium) and prolactin [LTH (luteotropic hormone)] were purchased from Sigma–Aldrich Denmark (Brøndby, Denmark). FBS (foetal bovine serum), MEM non-essential amino acids (100 times) solution, penicillin–streptomycin [10000 units of penicillin (base) and 10000 μg of streptomycin (base)/ml)] and L-glutamine 200 mM (100 times) liquid were from Invitrogen (Taastrup, Denmark). Actrapid-Insulin was from Novo Nordisk (Bagsværd, Denmark). Cortisol was from SERVA Electrophoresis (Heidelberg, Germany). Sterile Femtotips for microinjection and Femtotip microloaders (2–20 μl) were from Eppendorf (Hamburg, Germany). The organelle-specific fluorescent markers glibenclamide-BODIPY® (4,4-difluoro-4-bora-3a,4a-diaza-*s*-indacene), MitoTracker Red CM-H_2XRos, LysoTracker Red DND-99, BODIPY® 493/503 neutral lipid stain and BOPIPY® C_5-ceramide complexed to BSA were from Molecular Probes (Eugene, OR, U.S.A.). Badan (6-bromoacetyl-2-dimethylaminonaphthalene) was from AnaSpec (San Jose, CA, U.S.A.).

Site-directed mutagenesis, protein expression, purification and badan labelling

Protein expression, purification and badan labelling of K50C-ACBP and of M24C-ACBP to produce FACI-50 and FACI-24 respectively were carried out as previously described [23].

A variant of FACI-50 was constructed by introducing two additional amino acid substitutions, Y28F and K32A, into the existing K50C-ACBP plasmid. Site-directed mutagenesis was carried out as previously described [24]. The primers used for amplification of mutant bovine ACBP were 5′-GTAGTGAGA-GAAGATGAACAACATTTC-3′ upstream (Y28F) and 5′-GCT-CAAGCTACCGTTGGTGACATCAAC-3′ downstream (K32A). Underlined bases indicate substitutions. Protein expression, purification and badan labelling of bovine Y28F/K32A/K50C-ACBP to produce Y28F/K32A-FACI-50 were carried out as for FACI-50 [23].

Ligand binding studies of FACI-24, FACI-50 and Y28F/K32A-FACI-50

Dissociation constants of FACI-24, FACI-50 and Y28F/K32A-FACI-50 were determined by isothermal microcalorimetry essentially as described previously [25], except that the buffer used was 20 mM Mes and 100 mM NaCl (pH 6.8).

Cell culture

HeLa cells were cultured in T_{75}-culture flasks in DMEM with penicillin (50 units/ml), streptomycin (50 μg/ml) ($DMEM_{pen/strep}$), 10 % (v/v) FBS, 0.1 mM non-essential amino acids and 10 mM L-glutamine, in a humidified incubator at 37 °C in the presence of 5 % CO_2. Medium was exchanged every 2 days and the cells were subcultured at pre-confluent densities using 0.25 % (w/v) trypsin and 0.03 % (w/v) EDTA in PBS (pH 7.4) (trypsin/EDTA solution).

The BMGE cells originated from [26] and were kindly provided by Professor Karsten Kristiansen (University of Southern Denmark, Odense, Denmark). BMGE cells were cultured in T_{75}-culture flasks in $DMEM_{pen/strep}$ supplemented with 20 % (v/v) FBS, 10 mM L-glutamine and insulin, cortisol and prolactin (1.0 μg/ml each) in a humidified incubator at 37 °C in the presence of 5 % CO_2 [26–28]. Cells were subcultured at pre-confluent densities using trypsin/EDTA solution as described above.

Establishment of stable HeLa cell lines expressing GFP (green fluorescent protein) or GFP–ACBP

The expression vector pEGFP-C1 with and without bovine liver ACBP inserted were obtained from Professor Karsten Kristiansen (University of Southern Denmark). On the day before transfection, HeLa cells (2–6 × 10^6 cells) were plated on to 60 mm culture Petri dishes containing 4 ml of DMEM supplemented with 10 % FBS and without antibiotics. HeLa cells were transfected with ACBP–GFP vector or empty vector by using Lipofectamine™ Plus Reagent (Gibco Life Technologies, Rockville, MD, U.S.A.). The transfection procedure was based on the manufacturers' protocol and adapted to 60 mm Petri dishes.

The transfected cell populations were maintained in complete DMEM supplemented with 0.5 mg/ml G418, and cells were split at a ratio of 1:10 twice a week. Cells transfected with expression vector alone served as controls. For imaging experiments, cells were grown on glass-bottom Petri dishes (MatTek).

Microinjection of HeLa and BMGE cells

For microinjection experiments, cells that had been grown to subconfluence were dissociated from the plates by treatment with trypsin/EDTA solution for 5 min at 37 °C. An aliquot of 1 × 10^5 cells was plated on to 50 mm diameter glass-bottom culture dishes (MatTek) and cultured to 70–80 % confluence in culture medium. Immediately before microinjection, the medium was removed and replaced by C-Hepes buffer (20 mM Hepes, 140 mM NaCl, 5.5 mM glucose, 5 mM KCl, 1 mM NaH_2PO_4 and 1 mM $MgSO_4$, pH 7.4) pre-equilibrated to 37 °C. Microinjection was performed at room temperature (20 °C) using a microinjection system consisting of an Eppendorf Microinjector 5242 and a Micromanipulator 5170 (Eppendorf) attached to the side of a Leica DMIRBE inverted microscope (Leica Microsystems, Wetzlar, Germany). Microinjection was performed using a ×40 objective. HeLa and BMGE cells were microinjected with 200 and 400 μM respectively of FACI-50 or Y28F/K32A-FACI-50 dissolved in PBS (pH 7.4). The FACI solutions were centrifuged (20000 ***g***, 10 min and 4 °C) immediately before use. Sterile Femtotips (Eppendorf) were back-filled with 2 μl of the FACI solutions using Microloader tips (Eppendorf) and placed with a 45° angle over the Petri dish. Injection was executed with the automatic inject function of the system, while injection time was set to 0.5 s. The compensation pressure was set to 25 hPa and injection pressure was adjusted to 100 hPa for HeLa cells and 130 hPa for BMGE cells respectively.

Double labelling experiments by confocal and two-photon laser excitation microscopy

Microscopy was performed on a confocal microscope (model LSM 510 META; Carl Zeiss MicroImaging, Jena, Germany) using a ×40/1.2 NA (numerical aperture) Plan Apochromat water-immersion lens unless otherwise stated. Acquisition was performed using LSM 510 version 3.0 software (Carl Zeiss MicroImaging).

For transfected cells, GFP fluorescence was excited at 488 nm with a 30 mW Argon/2 laser, and images were collected using a primary HFT 488 dichroic beam splitter and a 505 nm long pass filter. The nuclei of GFP-transfected cells were identified by

incubating cells for 60 min with 16 μM DAPI (4′,6-diamidino-2-phenylindole) dissolved in C-Hepes buffer.

For FACI experiments, the 50 mm glass-bottom culture dishes were, immediately after microinjection, transferred to a heated (37.5 °C) microscope stage (TempControl Digital 37-2 device; Warner Instruments) with a custom-made aluminium insert to fit the 50 mm glass-bottom culture dishes. FACI-injected cells were identified by shortly switching on/off a blue reflector by which FACI-positive cells exhibited a bright green appearance.

For image acquisition, blue fluorophores (DAPI and FACIs) were excited using two-photon excitation laser scanning microscopy. Excitation was provided by a tuneable, broadband, mode-locked titanium–sapphire Mai Tai laser (Spectra-Physics Lasers) at 800 nm, which was reflected by a primary HFT KP 650 dichroic mirror, fluorescence was filtered with a secondary NFT 490 dichroic mirror, and emission was recorded with a 435–485 nm band-pass filter.

The ER was labelled by incubating cells with 2 μM glibenclamide-BODIPY® in C-Hepes buffer at 37 °C in 5 % CO_2 for 30 min.

The Golgi complex was identified with BOPIPY® C_5-ceramide (Molecular Probes) as follows: cells were incubated with 5 μM BODIPY® C_5-ceramide complexed to BSA in C-Hepes buffer for 30 min at 37 °C. Cells were then washed with C-Hepes buffer and incubated in $DMEM_{pen/strep}$ with serum for further 30 min at 37 °C.

Mitochondria were visualized using MitoTracker Red CM-H_2XRos with a final concentration of 0.5 μM in $DMEM_{pen/strep}$ culture medium without serum. Cells were labelled for 45 min at 37 °C in 5 % CO_2.

Labelling of lysosomal vesicles was performed by incubating cells with 75 nM LysoTracker Red DND-99 in $DMEM_{pen/strep}$ without serum at 37 °C in 5 % CO_2 for 30 min.

Image acquisitions of glibenclamide-BODIPY®, BODIPY® C_5-ceramide, MitoTracker Red CM-H_2XRos and LysoTracker Red DND-99 were performed with excitation at 543 nm provided by a 1 mV Helium/Neon1 (HeNe/1) laser, and emission was collected using a primary HFT488/543/633 dichroic beam splitter, a secondary NFT 545 dichroic mirror and a 565–615 nm band-pass filter.

Lipid droplets and endogenous membranes were identified using BODIPY® 493/503 neutral lipid stain. Labelling was performed by incubating cells with 10 μg/ml of this lipophilic dye dissolved in C-Hepes at 37 °C in 5 % CO_2 for 45 min. For imaging, BODIPY® 493/503 was excited at 488 nm using a 30 mV Argon/2 laser and emission was collected using a primary HFT 488 dichroic beam splitter and a 500–530 IR band pass filter.

For double labelling experiments, the two channels were scanned alternately in a line-by-line fashion, having only one laser line and one detector channel on at each time. Acquisition of confocal fluorescence images was performed using a pinhole diameter corresponding to 1 Airy unit unless otherwise stated. Images were assessed using the LSM Browser (Carl Zeiss MicroImaging) and processed using ImageJ open-source software (http://rsb.info.nih.gov/ij).

Quantitative co-localization analysis

Co-localization of FACI-50 or Y28F/K32A-FACI-50 respectively with organelle-specific dyes was performed using the ICA (intensity correlation analysis) method described by Li et al. [29]. The ICA method tests for co-localization by comparing how the intensity of two signals varies with respect to each other, i.e. it tests their synchrony. With random staining, the ICQ (intensity correlation quotient) is ~ 0; for dependent staining $0 < \mathrm{ICQ} \leqslant +0.5$, whereas for segregated staining $0 > \mathrm{ICQ} \geqslant -0.5$ [29]. Pre-existing defined immunofluorescence images of random, dependent and segregated staining respectively were used as controls.

PDM (product of the differences from the mean), i.e. for each pixel, is defined as (Channel 1 intensity–Mean channel 1 intensity) × (Channel 2 intensity–Mean channel 2 intensity), which is equal to the $(A–a) \times (B–b)$ described by Li et al. [29]. ICA plots represent the fluorescence intensities of one channel as a function of the respective PDM values of both recording channels.

The software for quantitative co-localization analysis was provided as a plug-in (written by Elise Stanley, Toronto, ON, Canada) to ImageJ.

FACI-50 GP (generalized polarization) measurements

The fluorescence emission properties of FACI-50 are sensitive to the polarity of the local environment of the fluorescent probe badan. Saturating amounts of CoA shift the maximum emission yield of FACI-50 from 510 to 490 nm; acyl-CoA binding, in contrast, causes a red-shift of FACI-50 emission [22]. Emission spectral changes can be quantified comparing the GP values for shifted and unshifted fluorescence intensity peaks of FACI-50. GP values were calculated by: $\mathrm{GP} = I_b - I_g / I_b + I_g$, where I_b and I_g correspond to the intensities at the blue and green edges of the emission spectrum respectively [30,31]. *In vitro* fluorescence spectra were measured using a Chronos ISS fluorimeter (ISS, Champaign, IL, U.S.A.) with a λ_{ex} (excitation wavelength) of 374 nm using a laser diode as the excitation source. I_b and I_g were measured at 470 and 520 nm respectively. Two-photon excitation (800 nm) GP images of FACI-50-microinjected BMGE cells in C-Hepes buffer covering 435–465 and 535–565 nm range respectively were obtained simultaneously in dual-channel set-up on a confocal microscope (model LSM 510 META; Carl Zeiss MicroImaging). The objective used was a ×40/1.2 NA Plan Apochromat water-immersion objective. The two images were analysed using SimFCS software (Laboratory for Fluorescence Dynamics) to obtain the GP image and the associated GP histogram (distribution of the GP values per pixel).

Effect of defatted BSA and fatty acid addition on ACBP localization

FACI-50-microinjected BMGE cells prelabelled with BODIPY® C_5-ceramide as described above were incubated for 10 min in C-Hepes buffer containing 600 μM FAFBSA (fatty-acid-free BSA) or BSA complexed with 2.66 mM OA (oleic acid) (OA–BSA) to give an OA/BSA molar ratio of 4.44, resulting in a free OA concentration [FFA_{OA}] of 150 nM as described previously [32,33]. The OA–BSA complexes were made by mixing stock solutions of 1.0 mM FAFBSA solution in C-Hepes with 50 mM OA sodium salts dissolved in C-Hepes to give a final BSA and OA concentration of 600 μM and 2.66 mM respectively (OA/BSA ratio of 4.44) [33].

Two-photon excitation FRAP (fluorescence recovery after photobleaching) experiments

To measure the mobility of FACI-50 in the Golgi complex of BMGE cells treated with FAFBSA or the OA–BSA complexes for 30 min, FRAP experiments were performed essentially as described in [34]. Fluorescence recovery curves were fitted using SigmaPlot scientific graphing software (Jandel Scientific, San Rafael, CA, U.S.A.) and half-time recoveries were calculated as described in [35].

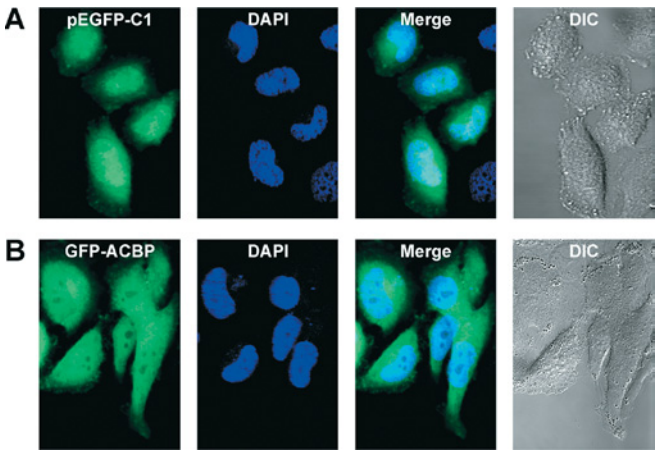

Figure 1 GFP–ACBP and GFP localization *in vivo* in HeLa cells

HeLa cells were stably transfected with the empty pEGFP-C1 vector (**A**) or GFP–ACBP (**B**). GFP fluorescence was excited at 488 nm with a 30 mW Argon/2 laser and images were collected using a primary HFT 488 dichroic beam splitter and a 505 nm long pass filter. The nuclei of GFP-transfected cells were identified by incubating cells for 60 min with 16 μM DAPI dissolved in C-Hepes buffer. DAPI was excited at 800 nm using two-photon excitation, which was reflected by a primary HFT KP 650 dichroic mirror, fluorescence was filtered with a secondary NFT 490 dichroic mirror, and emission was recorded with a 435–485 nm band-pass filter. DIC, differential interference contrast. All cell images were taken at 40× magnification as described in the Experimental section.

CD spectroscopy

Far-UV CD spectra of recombinant bovine L-ACBP, FACI-50, FACI-24 and Y28F/K32A-FACI-50 were recorded on a Jasco J-810 spectropolarimeter scanning wavelengths in the range 250–190 nm, averaging over 4–6 scans per experiment, data pitch of 0.1 nm and scan rate 20 nm/min at room temperature. Total protein concentration was 10 μM and the proteins were diluted from stocks into either Milli-Q water or 10 mM NaH_2PO_4 (pH 7.4). The cuvettes used were 0.1 cm Quartz-Suprasil from Hellma. Reference spectra of buffer or water were recorded during each session and subtracted accordingly. Each sample was allowed at least 10 min to reach equilibrium before spectrum acquisition.

RESULTS

A GFP–ACBP fusion protein expressed in HepG2 cells was found to localize both to the cytoplasm and to the nucleus [21]. However, no GFP expression control was reported in these experiments. We explored the possibility of using stable expression of GFP–ACBP to map the intracellular localization of ACBP in HeLa cells. The results showed that localization of the GFP–ACBP cannot be distinguished from that of GFP on its own (Figure 1). This shows that the GFP–ACBP fusion is unsuitable for studying the intracellular localization of basal 82–92-residue ACBP *in vivo*. There might be several reasons for this. First, GFP in itself is ~3.0 times larger than the ACBP and might therefore physically hinder interaction of the ACBP–GFP fusion protein with potential ACBP interaction partners. Secondly, GFP on its own has been show to target to organelles including the nucleus [36]. This could, if GFP is the dominating part of the fusion protein, provide misleading results.

ACBP localizes to the ER and Golgi complex in HeLa cells

Fluorescence emission of FACI-50-injected HeLa cells shows that bovine FACI-50 is highly concentrated close to the nucleus, with moderate fluorescence intensity of the perinuclear membrane typical for the localization to the Golgi and ER (results not shown). The nucleus itself and the remaining cytosol show much lower fluorescence emission intensities. Co-staining of FACI-50-microinjected HeLa cells with the ER marker glibenclamide-BODIPY® or the structural Golgi marker BODIPY® C_5-ceramide strongly indicates co-localization of ACBP both to the ER and to the Golgi, with an ICQ of 0.193 and 0.135 respectively.

Although the sequences of bovine and human L-ACBP show 94% identity, it could be argued that the use of a bovine L-ACBP-based probe in the human-derived HeLa cell line is non-physiological. We therefore switched to the BMGE cell line.

Localization of ACBP to the ER and Golgi complex of BMGE cells is ligand-dependent

In contrast with HeLa cells, BMGE cells represent a much more homogeneously shaped cell population. BMGE cells are morphologically large, very flat cells and, in the light microscope, the nucleus and surrounding membranous organelles can be clearly distinguished from the remaining cytosol. This makes delivery of FACI-50 into the cytosol by microinjection easier compared with HeLa cells, and thus significantly reduces the risk of injection of the fluorescent probe into or near the nucleus, which could lead to incorrect interpretation of ACBP localization results.

Microinjection of FACI-50 into BMGE cells confirms that ACBP localizes to the ER and Golgi, as seen in HeLa cells (Figures 2A and 3A). In contrast, we were unable to show co-localization of FACI-50 with mitochondria, lysosomes or fat droplets when microinjection of FACI-50 into BMGE cells incubated with MitoTracker Red CM-H_2XRos, LysoTracker Red DND-99 or the neutral lipid stain BODIPY® 493/503 respectively was performed (see Supplementary Figures 1–3 at http://www.BiochemJ.org/bj/410/0463/bj4100463add.htm). In order to test the importance of ligand binding for association of ACBP with the ER/Golgi, we produced by site-directed mutagenesis an FACI-50 variant with impaired ligand binding ability, Y28F/K32A-FACI-50. The Y28F/K32A site-directed mutations in yeast ACBP have previously been shown to reduce dodecanoyl-CoA binding of native bovine ACBP by approx. 1000-fold (J.S. Hansen, N.J. Færgeman, B.B. Kragelund and J. Knudsen, unpublished work).

Isothermal titration microcalorimetry of FACI-24, FACI-50 and Y28F/K32A-FACI-50 determined the dissociation constant (K_d) of myristoyl-CoA binding to FACI-24 and FACI-50 to be 62 ± 25 nM ($n = 2$) and 177 ± 52 nM ($n = 3$) respectively. However, Y28F/K32A-FACI-50 could not be shown to bind myristoyl-CoA at all (results not shown). Fold integrity of all three FACI variants was confirmed from far-UV CD spectral analysis (see Supplementary Figure 4 at http://www.BiochemJ.org/bj/410/0463/bj4100463add.htm), demonstrating that the effect from mutations and fluorescence labelling was directly on ligand binding and clearly not on structure. The disruption of ligand binding activity strongly perturbed the intracellular localization of ACBP, resulting in an even distribution of Y28F/K32A-FACI-50 throughout the whole cell including the nucleus (Figures 2B and 3B). The ICQs for co-localization between ER staining and FACI-50 and Y28F/K32A-FACI-50 staining were 0.30 and 0.038 respectively, and between the Golgi and FACI-50 and Y28F/K32A-FACI-50 staining were 0.28 and −0.15 respectively. The low (0.038) or negative (−0.15) ICQs for co-staining of Y28F/K32A-FACI-50 with the ER or with the Golgi respectively show that association of the mutant protein with the ER is random and that it is segregated from the Golgi. This suggests that ligand binding targets ACBP to the ER/Golgi.

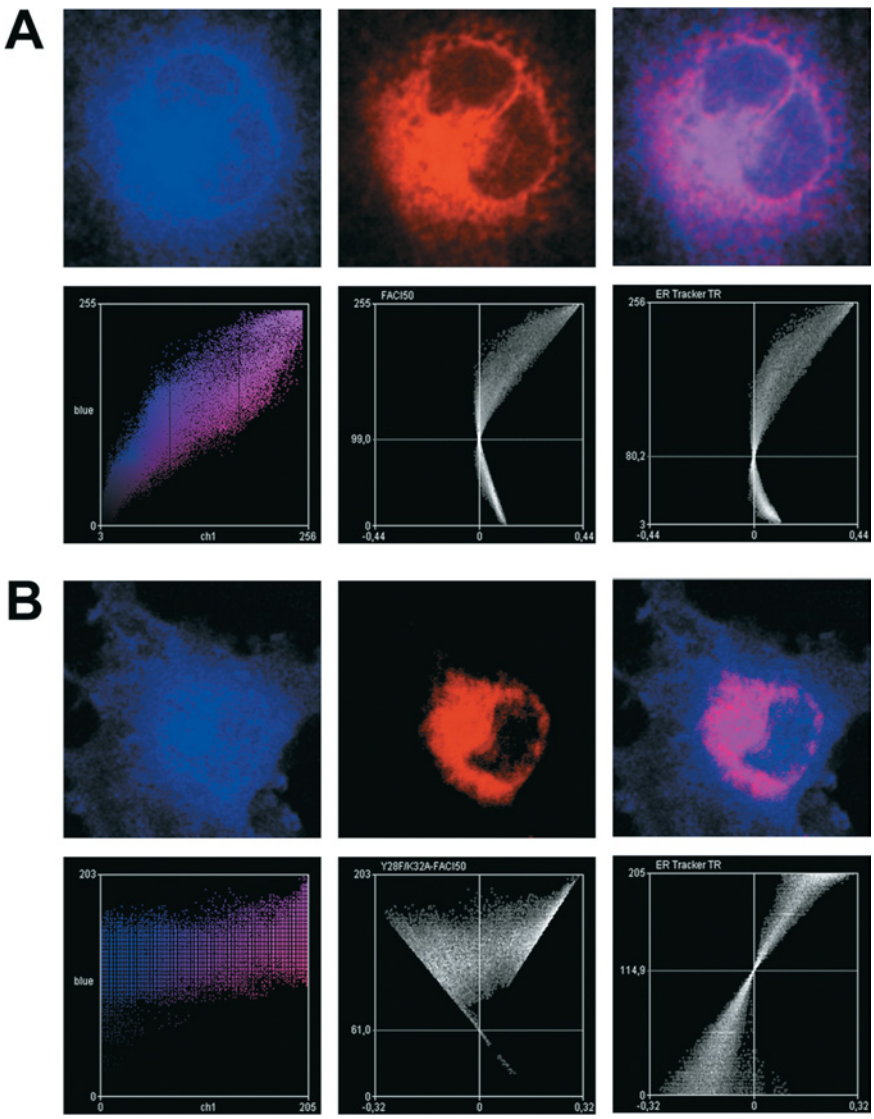

Figure 2 ACBP localization with the ER in BMGE cells is function-dependent

Localization of microinjected FACI-50 (**A**, upper left panel) or Y28F/K32A-FACI-50 (**B**, upper left panel) and ER tracker glibenclamide-BODIPY® (**A**, **B**, upper middle panel), in BMGE cells. Merged images are presented in upper right panels. Lower left panels show scatter plot of FACI-50 (**A**) and Y28F/K32A-FACI-50 (**B**) pixel staining intensities against ER tracker glibenclamide-BODIPY® pixel staining intensities. Lower middle and right panels show individual fluorescence intensities of FACI-50 (**A**, lower middle panel), Y28F/K32A-FACI-50 (**B**, lower middle panel) or glibenclamide-BODIPY® (lower right panels) plotted against their respective PDM values of both recording channels.

If this hypothesis holds, it should be possible to obtain similar changes in FACI-50 intracellular localization by manipulating the intracellular concentration of acyl-CoA levels. The intracellular concentration of free fatty acids and acyl-CoA is strongly affected by the concentration of free fatty acids in the media [32,37]. We therefore performed ICA measurements on FACI-50 co-localization with the ER and Golgi in cells pre-incubated with either FAFBSA or OA–BSA (molar ratio 4.44) in order to deplete or overload respectively the cells with fatty acids. Addition of FAFBSA to the medium caused a reduction in the ICA coefficient for FACI-50 co-localization/association with the Golgi marker from 0.128 ± 0.011 to 0.088 ± 0.009. On the contrary, addition of OA–BSA resulted in an increased ICA coefficient for FACI-50 association with the Golgi from 0.088 ± 0.009 to 0.190 ± 0.013 (Figure 4). This observation further supports the notion that ligand binding is essential for targeting of ACBP to the Golgi. It should be noted that the apparent overall lower ICQ of co-staining BMGE cells with FACI-50 and BOPIPY® C_5-ceramide in the BSA and OA–BSA challenging experiments was due to an 8-fold increase in image acquisition scan times, which reduces photobleaching of the fluorophores but also lowers the image resolution.

To exclude the possibility that the ligand-dependent FACI-50–Golgi interaction could be caused by the presence of badan on the surface of FACI-50 in the ligand-bound state, the experiments reported in Figure 4 were repeated with FACI-24, in which the fluorophore is buried underneath acyl-CoA in the holo-ACBP complex. FACI-24 exhibited the same ligand-dependent interaction with the Golgi as FACI-50 (results not shown), excluding that the FACI-50–acyl-CoA interaction with the Golgi is caused by the badan side chain.

GP measurements of FACI-50 *in vivo*

Bovine L-ACBP binds free CoA with approx. 1000-fold lower affinity ($K_d \approx 2\ \mu$M [38]) than it binds palmitoyl-CoA (2–8 nM [39]). Binding of CoA to FACI-50 causes a down-shift in

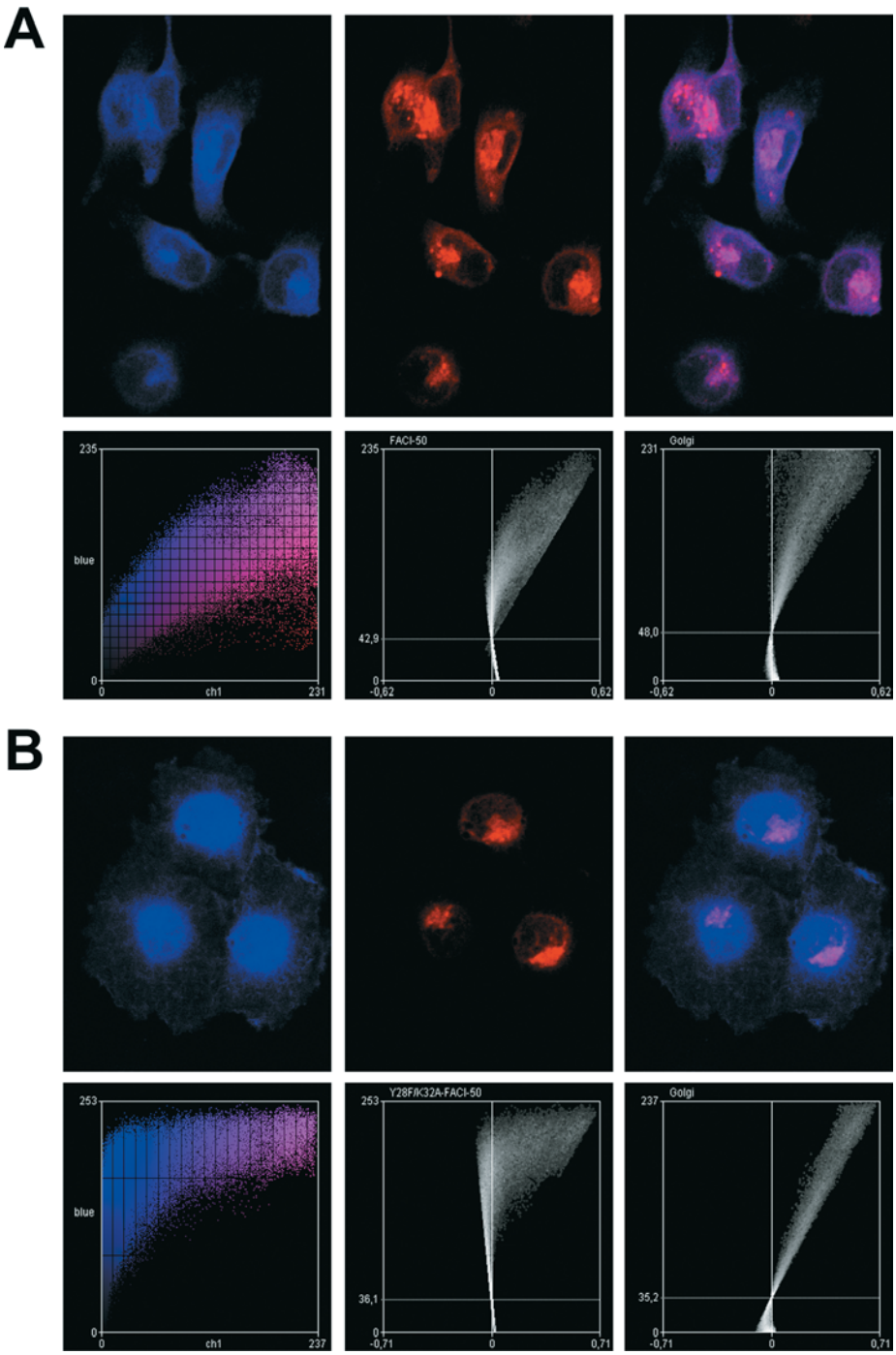

Figure 3 ACBP localizes to the Golgi in a ligand-binding-dependent manner

Localization of microinjected FACI-50 (**A**, upper left panel), Y28F/K32A-FACI-50 (**B**, upper left panel) and the Golgi marker BODIPY® C_5-ceramide (**A**, **B**, upper middle panel) in BMGE cells. Merged images are presented in the upper right panels. Lower left panels show scatter plots of FACI-50 (**A**) and Y28F/K32A-FACI-50 (**B**) pixel staining intensities against the Golgi marker BODIPY® C_5-ceramide pixel staining intensities. Lower middle and right panels show individual fluorescence intensities of FACI-50 (**A**, lower middle panel), Y28F/K32A-FACI-50 (**B**, lower middle panel) or the Golgi marker BODIPY® C_5-ceramide (lower right panels) plotted against their respective PDM values of both recording channels.

fluorescence emission maximum from 510 to 490 nm (Figure 5 and [22]). However, FACI-50 and FACI-50/oleoyl-CoA emission spectra could not be differentiated. The calculated GP values for the apo-FACI-50, FACI-50/oleoyl-CoA and FACI-50/CoA *in vitro* spectra recorded in Figure 5 were -0.361 ± 0.001, -0.375 ± 0.004 and -0.004 ± 0.002 respectively. Therefore GP measurements can be used to distinguish between FACI-50/CoA and apo-FACI-50 plus acyl-CoA/FACI 50. The determined *in vivo* GP value of -0.401 (Figure 5) was in the same range as *in vitro* GP values of apo-FACI-50 (-0.361) and oleoyl-CoA/FACI-50 (-0.375) respectively and significantly different from the *in vitro* FACI-50/CoA GP value. This strongly suggests

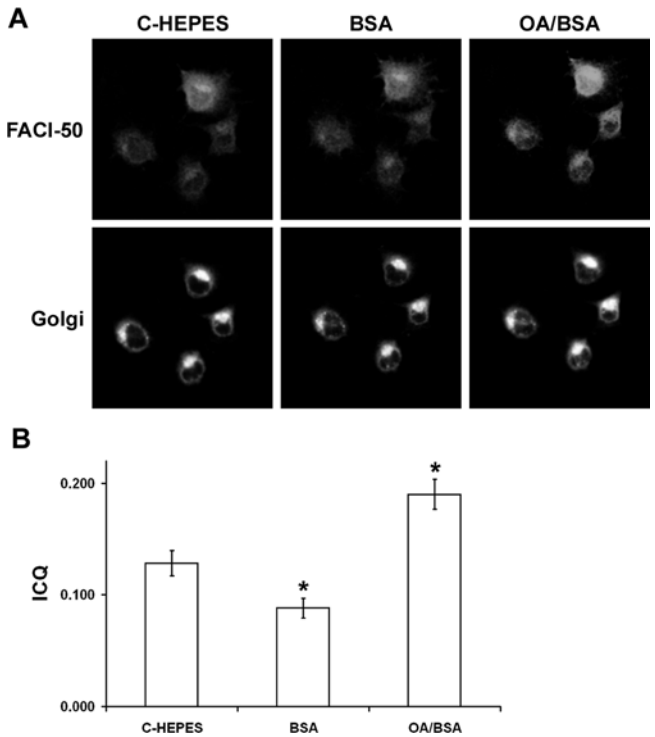

Figure 4 FAFBSA and OA–BSA challenging of FACI-50-injected BMGE cells

(**A**) FACI-50 (upper panels) and the Golgi marker BODIPY® C_5-ceramide (lower panels) localization in BMGE cells incubated successively for 10 min in C-Hepes buffer (left), C-Hepes buffer containing FAFBSA (600 μM) and in C-Hepes buffer containing OA–BSA (molar ratio 0.6/2.64 mM, to give a calculated free OA concentration of 150 nM [32,33]). (**B**) The Figure shows the ICQ values for FACI-50 fluorescence correlation with Golgi staining under the conditions described above. Results are means $\pm$ S.D. ($n = 5$). Asterisk indicates statistically significant differences ($P < 0.001$) between ICQ values obtained for cells in C-Hepes/FAFBSA buffer relative to the same cells incubated in C-Hepes buffer and C-Hepes/OA–BSA buffer respectively.

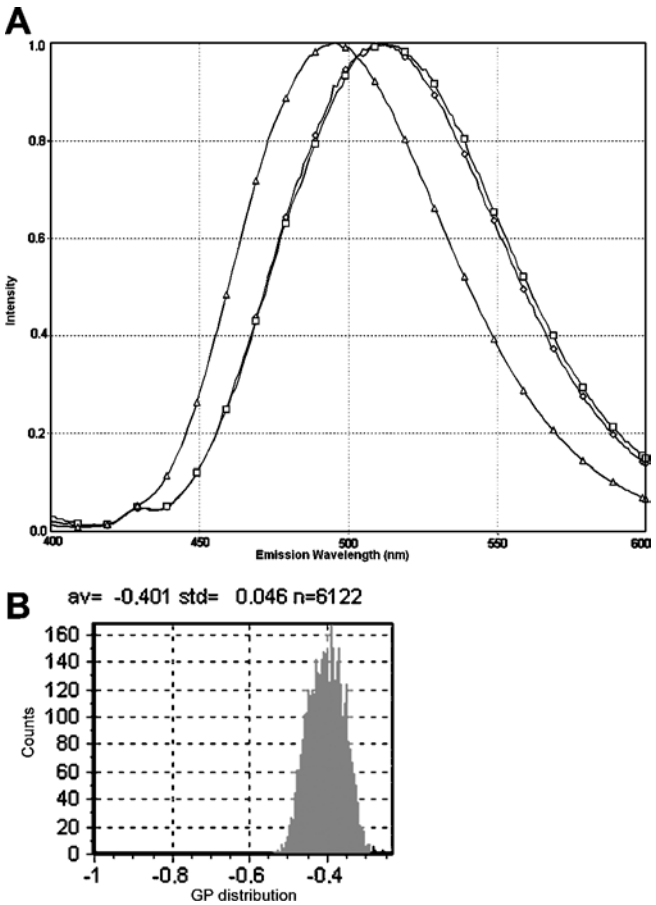

Figure 5 Normalized FACI-50 spectra and GP measurements in BMGE cells

(**A**) Normalized emission spectra of 1 μM FACI-50 in the absence (open squares) or presence of saturating amounts of CoA (open triangles) or oleoyl-CoA (open diamonds). (**B**) Histogram of whole cell GP measurements in FACI-50-injected BMGE cells.

that ACBP *in vivo* is present as either apo-ACBP or acyl-CoA–ACBP and not in complexes with CoA.

ACBP mobility in the Golgi is highly affected by endogenous fatty acid levels

The fact that addition of OA–BSA to the incubation medium results in increased co-localization with the Golgi (Figure 4), combined with the fact that disruption of ligand binding capability segregates FACI-50 from the Golgi, confirms the hypothesis that ligand binding is essential and targets ACBP to the Golgi. This notion is further supported by FRAP analysis, which showed that the fluorescence recovery half-time of FACI-50 in the Golgi complex of BMGE cells increased from 0.8 ± 0.4 s in C-Hepes buffer to 3.7 ± 0.6 s in C-Hepes plus OA–BSA in the culture medium (Figure 6). FRAP experiments on FACI-50-injected BMGE cells incubated with FAFBSA did not alter ACBP mobility compared with cells incubated in C-Hepes buffer alone (results not shown). A 5-fold reduction in FACI-50 mobility in the presence of OA–BSA in the culture medium strongly suggests that acyl-CoA binding targets FACI-50 to the Golgi and that FACI-50 is actually transiently associated with the Golgi.

DISCUSSION

Previous experimental data of the intracellular distribution of ACBP using indirect immunofluorescence or immunogold electron microscopy have, as pointed out in the Introduction section, yielded variable results from ACBP being exclusively cytosolic in Leydig cells [11–13] or found in the nucleus only of undifferentiated 3T3-L1 pre-adipocytes or in both the nucleus and cytosol of differentiated 3T3-L1 cells [21]. In other cells, including rat testes Leydig, Sertoli and seminiferous tubule cells, ACBP distributed over the whole cytosol, but was also found at the smooth ER, Golgi and outer membrane of mitochondria [12]. In some cells, such as rat Stilling's cells, ACBP was concentrated around large cytoplasmic vesicles [17]. The value of these previous experimental data may be questioned also due to the technical problems mentioned above.

In the present study, we circumvented these difficulties by performing live-cell imaging on microinjected fluorescently labelled ACBP in HeLa and BMGE cells. The results show that although ACBP was found throughout the whole cell, including in the nucleus, it distributes in a very heterogeneous manner. ACBP was found to be highly enriched on the ER, Golgi and the perinuclear membrane, with lower concentrations seen in the cytosol and in the nucleus, a finding that is in agreement with what has previously been found by indirect immunohistochemistry in rat hepatoma cells [7] and L-cell fibroblasts [20]. The co-localization of FACI-50 with both the ER and Golgi was confirmed by co-staining FACI-50-injected cells with organelle-specific stains of these two compartments and calculating the ICQ

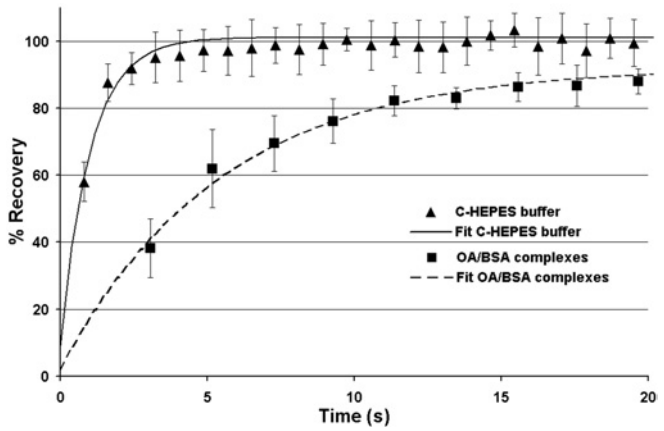

Figure 6 FRAP of FACI-50 in the Golgi

An image was acquired of FACI-50-injected BMGE cells in C-Hepes buffer and cells were incubated for 20 min with OA–BSA buffer (molar ratio 0.6/2.64 mM) respectively. A region of interest (ROI) of the Golgi was photobleached for a very brief period by two-photon laser excitation (45 % output) at 800 nm. Images were taken at different time points after photobleaching to monitor the fluorescence recovery. After background correction, the ratio of the fluorescence intensity in a photobleached region to the fluorescence intensity of the whole cell was calculated for each time point. This ratio was divided by the corresponding ratio obtained from the prebleaching image and presented as the percentage recovered. Each data point, derived from an average of five experiments, was fitted to the equation $y = y_0 + a(1 - e^{-kt})$, where k is the rate constant, by using SigmaPlot scientific graphing software. Values are means $\pm$ S.D. ($n = 5$). Half-time recoveries ($t_{1/2}$) were calculated according to $t_{1/2} = \ln(2)/k$.

between the FACI-50 and organelle dye emission fluorescence. The calculated ICQs for FACI-50 co-localization with the ER and Golgi stains in BMGE cells suggest strong interaction with both compartments. The Y28F/K32A-FACI-50 mutations, which disrupt myristoyl-CoA binding, but retain the overall three-dimensional structure of the protein, reduced the ICQ for co-localization between the ER and Golgi staining from 0.30 and 0.28 for FACI-50 respectively to 0.038 and -0.15 for Y28F/K32A-FACI-50 staining respectively, showing that Y28F/K32A-FACI-50 no longer associates with the ER and segregates from the Golgi. It has previously been shown that the intracellular concentration of free fatty acids and acyl-CoA is strongly affected by the concentration of free fatty acids in the media [32,37]. The present study shows that ACBP is likely to occur as apo-ACBP or ACBP–acyl-CoA, and not as ACBP–CoA complex *in vivo*. Increasing the cellular concentration of acyl-CoA would therefore be expected to increase the concentration of ACBP–acyl-CoA. If ligand binding is required to target ACBP to the ER and Golgi, it should be possible to alter ACBP association with the two organelles by manipulating the fatty acid concentration in the culture media. Our results show that this is indeed the case. Addition of FAFBSA to the BMGE cell culture media, which will extract fatty acids from the cells, reduced the ICQ for FACI-50 association with the Golgi from 0.12 to $\sim$0.09, whereas addition of OA–BSA increased the ICQ to $\sim$0.18 (Figure 4). The fact that addition of OA–BSA to the media, in addition to increasing the ICQ, also reduced the mobility of FACI-50 associated with the Golgi by 5-fold, as shown by FRAP experiments (Figure 6), strongly supports the perception that ligand binding targets ACBP to the Golgi.

The functional association of ACBP with both the ER and Golgi opens new windows for interpretations of ACBP function in relation to the existing published literature data. Long-chain acyl-CoA synthetase activity is predominantly found on microsomes (73 %), mitochondria (20 %) and in peroxisomes (7 %) [40], but not on the Golgi. Targeting of ACBP to the ER in a ligand-dependent manner would therefore make sense, since most of the acyl-CoA synthases and lipid-synthesizing acyltransferases are found on the ER. In this respect, it is interesting that ACBP has been shown to co-localize with ACAT (acyl-CoA:cholesterol acyltransferase) in the ER and perinuclear region in L-cell fibroblasts [20]. The Golgi has not been reported to contain acyl-CoA synthetase activity, but it has been reported to harbour lysophospholipid acyltransferases that have been suggested to co-ordinately regulate the Golgi membrane shape and tubule formation [41] as well as protein acylation [42]. These observations provide a possible explanation for the long-known requirement of acyl-CoA for vesicle fusion and budding [43–46]. The present result showing that ACBP gets targeted to the Golgi in a ligand-dependent manner makes acyl-CoA–ACBP a likely candidate for donating acyl-CoA esters required for budding and fusion. Previous data show that Acb1p (ACBP)-depleted yeast show all signs of perturbed vesicle trafficking, including: (i) accumulation of numerous small vesicles in the cytosol, (ii) appearance of fragmented vacuoles unable to fuse due to the lack of essential SNARE proteins, (iii) appearance of multilayered plasma membrane and (iv) induction of increased uptake of the accumulating vesicles in the vacuole by micro-autophagocytosis [4]. The observation that the *C. elegans* MAA-1 ACBP domain protein participates in plasma-membrane endosomal vesicle recycling confirms a role of ACBP proteins in donating acyl-CoA required for fusion and budding of vesicles [6].

ACBP does not contain any specific organelle-targeting sequences, except for a potential ER retrieval signal consisting of a di-lysine (KK) motif near the C-terminus [47]. However, this sequence motif is only conserved in a limited number of mammalian basal ACBP isoforms [48]. The present results show that this sequence motif on its own is unable to target bovine L-ACBP to the ER and Golgi and that ligand binding is essential and required to target FACI-50 to the Golgi. The actual mechanism by which ACBP attaches to the membrane is at present unknown. It has been reported that ACBP interacts with charged lipids in a membrane-curvature-dependent manner [49]. However, these experiments were carried out at very low ionic strength and cannot be repeated at physiological ionic strength by using isothermal titration calorimetry (J. S. Hansen, N. J. Færgeman, B. B. Kragelund and J. Knudsen, unpublished work). Recent results obtained by atomic force microscopy have shown that bovine L-ACBP–palmitoyl-CoA associates with DOPC (1,2-dioleoyl-*sn*-3-glycerophosphocholine) linear membranes [3]. A possible mechanistic explanation for this association could be an exchange of the palmitoyl-acyl chain of the ACBP-bound acyl-CoA with an oleoyl-acyl chain from a DOPC molecule in the membrane. This would leave the CoA head group bound in the binding site, with the palmitoyl-chain immersed in the DOPC bilayer, stabilized by the phosphocholine-oleoyl chain flipping out from the membrane and into the ACBP–acyl-CoA-binding site. The observation that two human L-ACBP molecules have the ability to share one intact dodecanoyl-CoA molecule having the head group bound in one ACBP and the acyl-chain in the other ACBP-binding site stabilized by a free fatty acid bound in one ACBP and a 4-phosphopanteteine fragment in the other ACBP [50] supports the above-suggested model for ACBP–acyl-CoA membrane binding. Alternatively, ACBP could interact with proteins residing in either the ER and/or the Golgi apparatus, which is currently being investigated.

This work was supported by a grant to J.K. from the Danish Natural Science Research Council. We thank Dr Louis Bagatolli (University of Southern Denmark) and Dr Daniel Wüstner (University of Southern Denmark) for advice and technical assistance concerning fluorescence microscopy.

REFERENCES

1 Burton, M., Rose, T. M., Faergeman, N. J. and Knudsen, J. (2005) Evolution of the acyl-CoA binding protein (ACBP). Biochem. J. **392**, 299–307
2 Rasmussen, J. T., Faergeman, N. J., Kristiansen, K. and Knudsen, J. (1994) Acyl-CoA-binding protein (ACBP) can mediate intermembrane acyl-CoA transport and donate acyl-CoA for beta-oxidation and glycerolipid synthesis. Biochem. J. **299**, 165–170
3 Cohen Simonsen, A., Bernchou Jensen, U., Faergeman, N. J., Knudsen, J. and Mouritsen, O. G. (2003) Acyl-coenzyme A organizes laterally in membranes and is recognized specifically by acyl-coenzyme A binding protein. FEBS Lett. **552**, 253–258
4 Faergeman, N. J., Feddersen, S., Christiansen, J. K., Larsen, M. K., Schneiter, R., Ungermann, C., Mutenda, K., Roepstorff, P. and Knudsen, J. (2004) Acyl-CoA-binding protein, Acb1p, is required for normal vacuole function and ceramide synthesis in *Saccharomyces cerevisiae*. Biochem. J. **380**, 907–918
5 Gaigg, B., Neergaard, T. B., Schneiter, R., Hansen, J. K., Faergeman, N. J., Jensen, N. A., Andersen, J. R., Friis, J., Sandhoff, R., Schroder, H. D. and Knudsen, J. (2001) Depletion of acyl-coenzyme A-binding protein affects sphingolipid synthesis and causes vesicle accumulation and membrane defects in *Saccharomyces cerevisiae*. Mol. Biol. Cell **12**, 1147–1160
6 Larsen, M. K., Tuck, S., Faergeman, N. J. and Knudsen, J. (2006) MAA-1, a novel acyl-CoA-binding protein involved in endosomal vesicle transport in *Caenorhabditis elegans*. Mol. Biol. Cell **17**, 4318–4329
7 Petrescu, A. D., Payne, H. R., Boedecker, A., Chao, H., Hertz, R., Bar-Tana, J., Schroeder, F. and Kier, A. B. (2003) Physical and functional interaction of acyl-CoA-binding protein with hepatocyte nuclear factor-4 alpha. J. Biol. Chem. **278**, 51813–51824
8 Barmack, N. H., Bilderback, T. R., Liu, H., Qian, Z. and Yakhnitsa, V. (2004) Activity-dependent expression of acyl-coenzyme A-binding protein in retinal Muller glial cells evoked by optokinetic stimulation. J. Neurosci. **24**, 1023–1033
9 Shulga, N. and Pastorino, J. G. (2006) Acyl coenzyme a binding protein augments bid-induced mitochondrial damage and cell death by activating μ-calpain. J. Biol. Chem. **281**, 30824–30833
10 Knudsen, J., Burton, M. and Færgeman, N. (2004) Long chain acyl-CoA esters and acyl-CoA binding protein (ACBP) in cell function. Adv. Mol. Cell Biol. **33**, 123–153
11 Rheaume, E., Tonon, M. C., Smih, F., Simard, J., Desy, L., Vaudry, H. and Pelletier, G. (1990) Localization of the endogenous benzodiazepine ligand octadecaneuropeptide in the rat testis. Endocrinology **127**, 1986–1994
12 Schultz, R., Pelto-Huikko, M. and Alho, H. (1992) Expression of diazepam binding inhibitor-like immunoreactivity in rat testis is dependent on pituitary hormones. Endocrinology **130**, 3200–3206
13 Duparc, C., Lefebvre, H., Tonon, M. C., Vaudry, H. and Kuhn, J. M. (2003) Characterization of endozepines in the human testicular tissue: effect of triakontatetraneuropeptide on testosterone secretion. J. Clin. Endocrinol. Metab. **88**, 5521–5528
14 Knudsen, J., Hojrup, P., Hansen, H. O., Hansen, H. F. and Roepstorff, P. (1989) Acyl-CoA-binding protein in the rat. Purification, binding characteristics, tissue concentrations and amino acid sequence. Biochem. J. **262**, 513–519
15 Alho, H., Varga, V. and Krueger, K. E. (1994) Expression of mitochondrial benzodiazepine receptor and its putative endogenous ligand diazepam binding inhibitor in cultured primary astrocytes and C-6 cells: relation to cell growth. Cell Growth Differ. **5**, 1005–1014
16 Johansson, O., Hilliges, M., Ostenson, C. G., Sandberg, E., Efendic, S. and Mutt, V. (1991) Immunohistochemical localization of porcine diazepam-binding inhibitor (DBI) to rat endocrine pancreas. Cell Tissue Res. **263**, 395–398
17 Lesouhaitier, O., Feuilloley, M., Lihrmann, I., Ugo, I., Fasolo, A., Tonon, M. C. and Vaudry, H. (1996) Localization of diazepam-binding inhibitor-related peptides and peripheral type benzodiazepine receptors in the frog adrenal gland. Cell Tissue Res. **283**, 403–412
18 Toranzo, D., Tong, Y., Tonon, M. C., Vaudry, H. and Pelletier, G. (1994) Localization of diazepam-binding inhibitor and peripheral type benzodiazepine binding sites in the rat ovary. Anat. Embryol. (Berlin) **190**, 383–388
19 Snyder, M. J. and Antwerpen, R. V. (1997) Cellular distribution, levels, and function of the diazepam-binding inhibitor/acyl-CoA-binding protein in last instar *Manduca sexta* midgut. Cell. Tissue Res. **288**, 177–184
20 Chao, H., Zhou, M., McIntosh, A., Schroeder, F. and Kier, A. B. (2003) ACBP and cholesterol differentially alter fatty acyl CoA utilization by microsomal ACAT. J. Lipid Res. **44**, 72–83
21 Helledie, T., Antonius, M., Sorensen, R. V., Hertzel, A. V., Bernlohr, D. A., Kolvraa, S., Kristiansen, K. and Mandrup, S. (2000) Lipid-binding proteins modulate ligand-dependent trans-activation by peroxisome proliferator-activated receptors and localize to the nucleus as well as the cytoplasm. J. Lipid Res. **41**, 1740–1751
22 Hansen, J. S., Villadsen, J. K., Gaster, M., Faergeman, N. J. and Knudsen, J. (2006) Micro method for determination of nonesterified fatty acid in whole blood obtained by fingertip puncture. Anal. Biochem. **355**, 29–38
23 Wadum, M. C., Villadsen, J. K., Feddersen, S., Moller, R. S., Neergaard, T. B., Kragelund, B. B., Hojrup, P., Faergeman, N. J. and Knudsen, J. (2002) Fluorescently labelled bovine acyl-CoA-binding protein acting as an acyl-CoA sensor: interaction with CoA and acyl-CoA esters and its use in measuring free acyl-CoA esters and non-esterified fatty acids. Biochem. J. **365**, 165–172
24 Fisher, C. L. and Pei, G. K. (1997) Modification of a PCR-based site-directed mutagenesis method. BioTechniques **23**, 570–574
25 Faergeman, N. J., Sigurskjold, B. W., Kragelund, B. B., Andersen, K. V. and Knudsen, J. (1996) Thermodynamics of ligand binding to acyl-coenzyme A binding protein studied by titration calorimetry. Biochemistry **35**, 14118–14126
26 Schmid, E., Franke, W. W., Grund, C., Schiller, D. L., Kolb, H. and Paweletz, N. (1983) An epithelial cell line with elongated myoid morphology derived from bovine mammary gland. Expression of cytokeratins and desmosomal plaque proteins in unusual arrays. Exp. Cell Res. **146**, 309–328
27 Rudland, P. S., Hallowes, R. C., Durbin, H. and Lewis, D. (1977) Mitogenic activity of pituitary hormones on cell cultures of normal and carcinogen-induced tumor epithelium from rat mammary glands. J. Cell Biol. **73**, 561–577
28 Schmid, E., Schiller, D. L., Grund, C., Stadler, J. and Franke, W. W. (1983) Tissue type-specific expression of intermediate filament proteins in a cultured epithelial cell line from bovine mammary gland. J. Cell Biol. **96**, 37–50
29 Li, Q., Lau, A., Morris, T. J., Guo, L., Fordyce, C. B. and Stanley, E. F. (2004) A syntaxin 1, $G\alpha_o$, and N-type calcium channel complex at a presynaptic nerve terminal: analysis by quantitative immunocolocalization. J. Neurosci. **24**, 4070–4081
30 Parasassi, T., De Stasio, G., Ravagnan, G., Rusch, R. M. and Gratton, E. (1991) Quantitation of lipid phases in phospholipid vesicles by the generalized polarization of Laurdan fluorescence. Biophys. J. **60**, 179–189
31 Tricerri, M. A., Toledo, J. D., Sanchez, S. A., Hazlett, T. L., Gratton, E., Jonas, A. and Garda, H. A. (2005) Visualization and analysis of apolipoprotein A-I interaction with binary phospholipid bilayers. J. Lipid Res. **46**, 669–678
32 Kampf, J. P. and Kleinfeld, A. M. (2004) Fatty acid transport in adipocytes monitored by imaging intracellular free fatty acid levels. J. Biol. Chem. **279**, 35775–35780
33 Richieri, G. V., Anel, A. and Kleinfeld, A. M. (1993) Interactions of long-chain fatty acids and albumin: determination of free fatty acid levels using the fluorescent probe ADIFAB. Biochemistry **32**, 7574–7580
34 Patterson, G. H. and Piston, D. W. (2000) Photobleaching in two-photon excitation microscopy. Biophys. J. **78**, 2159–2162
35 Hao, M., Mukherjee, S. and Maxfield, F. R. (2001) Cholesterol depletion induces large scale domain segregation in living cell membranes. Proc. Natl. Acad. Sci. U.S.A. **98**, 13072-13077
36 Gerdes, H. H. and Kaether, C. (1996) Green fluorescent protein: applications in cell biology. FEBS Lett. **389**, 44–47
37 Faergeman, N. J., Black, P. N., Zhao, X. D., Knudsen, J. and DiRusso, C. C. (2001) The acyl-CoA synthetases encoded within FAA1 and FAA4 in *Saccharomyces cerevisiae* function as components of the fatty acid transport system linking import, activation, and intracellular utilization. J. Biol. Chem. **276**, 37051–37059
38 Rolf, B., Oudenampsen-Kruger, E., Borchers, T., Faergeman, N. J., Knudsen, J., Lezius, A. and Spener, F. (1995) Analysis of the ligand binding properties of recombinant bovine liver-type fatty acid binding protein. Biochim. Biophys. Acta **1259**, 245–253
39 Fulceri, R., Knudsen, J., Giunti, R., Volpe, P., Nori, A. and Benedetti, A. (1997) Fatty acyl-CoA–acyl-CoA-binding protein complexes activate the Ca^{2+} release channel of skeletal muscle sarcoplasmic reticulum. Biochem. J. **325**, 423–428
40 Krisans, S. K., Mortensen, R. M. and Lazarow, P. B. (1980) Acyl-CoA synthetase in rat liver peroxisomes. Computer-assisted analysis of cell fractionation experiments. J. Biol. Chem. **255**, 9599–9607
41 Drecktrah, D., Chambers, K., Racoosin, E. L., Cluett, E. B., Gucwa, A., Jackson, B. and Brown, W. J. (2003) Inhibition of a Golgi complex lysophospholipid acyltransferase induces membrane tubule formation and retrograde trafficking. Mol. Biol. Cell **14**, 3459–3469
42 Fernandez-Hernando, C., Fukata, M., Bernatchez, P. N., Fukata, Y., Lin, M. I., Bredt, D. S. and Sessa, W. C. (2006) Identification of Golgi-localized acyl transferases that palmitoylate and regulate endothelial nitric oxide synthase. J. Cell Biol. **174**, 369–377
43 Glick, B. S. and Rothman, J. E. (1987) Possible role for fatty acyl-coenzyme A in intracellular protein transport. Nature **326**, 309–312
44 Ostermann, J., Orci, L., Tani, K., Amherdt, M., Ravazzola, M., Elazar, Z. and Rothman, J. E. (1993) Stepwise assembly of functionally active transport vesicles. Cell **75**, 1015–1025
45 Pfanner, N., Glick, B. S., Arden, S. R. and Rothman, J. E. (1990) Fatty acylation promotes fusion of transport vesicles with Golgi cisternae. J. Cell Biol. **110**, 955–961
46 Pfanner, N., Orci, L., Glick, B. S., Amherdt, M., Arden, S. R., Malhotra, V. and Rothman, J. E. (1989) Fatty acyl-coenzyme A is required for budding of transport vesicles from Golgi cisternae. Cell **59**, 95–102

47 Vincent, M. J., Martin, A. S. and Compans, R. W. (1998) Function of the KKXX motif in endoplasmic reticulum retrieval of a transmembrane protein depends on the length and structure of the cytoplasmic domain. J. Biol. Chem. **273**, 950–956
48 Burton, M., Rose, T. M., Faergeman, N. J. and Knudsen, J. (2005) Evolution of the acyl-CoA binding protein (ACBP). Biochem. J. **392**, 299–307
49 Chao, H., Martin, G. G., Russell, W. K., Waghela, S. D., Russell, D. H., Schroeder, F. and Kier, A. B. (2002) Membrane charge and curvature determine interaction with acyl-CoA binding protein (ACBP) and fatty acyl-CoA targeting. Biochemistry **41**, 10540–10553
50 Taskinen, J., van Aalten, D. M. F., Knudsen, J. and Wierenga, R. K. (2007) High resolution crystal structures of unliganded and liganded human liver ACBP reveal a new mode of binding for the acyl-CoA ligand. Proteins **66**, 229–238

Received 25 April 2007/4 October 2007; accepted 22 October 2007
Published as BJ Immediate Publication 22 October 2007, doi:10.1042/BJ20070559